



Cite this: *Phys. Chem. Chem. Phys.*,
2021, **23**, 18495

A molecular beam and computational study on the barrierless gas phase formation of (iso)quinoline in low temperature extraterrestrial environments†

Long Zhao,^a Matthew Prendergast,^a Ralf I. Kaiser,^{id}*^a Bo Xu,^b Wenchao Lu,^{id}^b Musahid Ahmed,^{id}*^b A. Hasan Howlader,^{id}^c Stanislaw F. Wnuk,^{id}*^c Alexander S. Korotchenko,^d Mikhail M. Evseev,^d Eugene K. Bashkirov,^d Valeriy N. Azyazov^{de} and Alexander M. Mebel^{id}*^c

Despite remarkable progress toward the understanding of the formation pathways leading to polycyclic aromatic hydrocarbons (PAHs) in combustion systems and in deep space, the complex reaction pathways leading to nitrogen-substituted PAHs (NPAHs) at low temperatures of molecular clouds and hydrocarbon-rich, nitrogen-containing atmospheres of planets and their moons like Titan have remained largely obscure. Here, we demonstrate through laboratory experiments and computations that the simplest prototype of NPAHs – quinoline and isoquinoline (C₉H₇N) – can be synthesized *via* rapid and de-facto barrier-less reactions involving *o*-, *m*- and *p*-pyridinyl radicals (C₅H₄N*) with vinylacetylene (C₄H₄) under low-temperature conditions.

Received 17th May 2021,
Accepted 5th August 2021

DOI: 10.1039/d1cp02169a

rsc.li/pccp

1. Introduction

During the last decade, significant progress has been made in untangling the fundamental elementary reactions leading to the gas phase formation of polycyclic aromatic hydrocarbons (PAHs) – organic molecules carrying fused benzene rings – with up to five six-membered rings through the exploitation of molecular beam experiments.^{1–14} In deep space, PAH-like molecules have been suggested to account for up to 30% of the galactic carbon budget^{15,16} and provide decisive nucleation sites for the formation of carbonaceous dust particles.¹⁷ From the spectroscopic viewpoint, PAH-like species have been also linked to the diffuse interstellar bands (DIBs) defined as discrete absorption features superimposed on the interstellar extinction curve ranging from the blue part of the visible (400 nm) to the near infrared (1.2 μm).¹⁸ Further, PAHs and their cations, anions, radicals, and partially (de)hydrogenated

counterparts are considered as carriers of the unidentified infrared (UIR) emission bands observed at 3.3, 6.2, 7.7, 11.2, and 12.7 μm;¹⁹ these emissions likely result from ultraviolet pumped infrared fluorescence of PAHs with an excess of 50 carbon atoms.^{19,20} The identification of the simplest PAH naphthalene (C₁₀H₈) along with chemically more complex PAHs such as anthracene/phenanthrene (C₁₄H₁₀) and pyrene/fluoranthene (C₁₆H₁₀) in some 20 carbonaceous chondrites^{21,22} along with isotope (D, ¹³C) studies²³ infers their extraterrestrial origin in circumstellar envelopes of carbon-rich asymptotic giant branch (AGB) stars such as of IRC + 10216 and possibly in planetary nebulae as their descendants. Overall, molecular beam experiments have revealed fundamental mass growth processes:^{14,24} (i) Hydrogen Abstraction – Acetylene Addition (HACA),^{3,10} (ii) Hydrogen Abstraction – Vinylacetylene Addition (HAVA),^{2,4,5,8} (iii) Phenyl Addition – Dehydro-Cyclization (PAC),⁷ (iv) Radical-Radical Reactions (RRR),¹ (v) Methylidyne Addition – Cyclization – Aromatization (MACA),²⁵ (vi) hydrogen-abstraction-methyl-addition,²⁶ (vii) clustering of hydrocarbons by radical-chain reaction (CHRCR),^{27–29} and (viii) aromatic α-alkynyl-linked hydrocarbon mechanism.³⁰ HAVA and MACA have no entrance barrier and are exoergic with all barriers involved ranging below the energy of the separated reactants. Consequently, these pathways have the capability to operate at low temperatures of cold molecular clouds such as TMC-1 and OMC-1 (10 K) and also in hydrocarbon rich atmospheres of planets and their moons like Titan and Pluto. These mechanistic concepts have provided a solid, experimentally

^a Department of Chemistry, University of Hawaii at Manoa, Honolulu, HI 96822, USA. E-mail: ralfk@hawaii.edu

^b Chemical Sciences Division, Lawrence Berkeley National Laboratory, Berkeley, CA 94720, USA. E-mail: mahmed@lbl.gov

^c Department of Chemistry and Biochemistry, Florida International University, Miami, FL 33199, USA. E-mail: wnuk@fiu.edu, mebel@fiu.edu

^d Samara National Research University, Samara 443086, Russian Federation

^e Lebedev Physical Institute, Samara 443011, Russian Federation

† Electronic supplementary information (ESI) available. See DOI: 10.1039/d1cp02169a

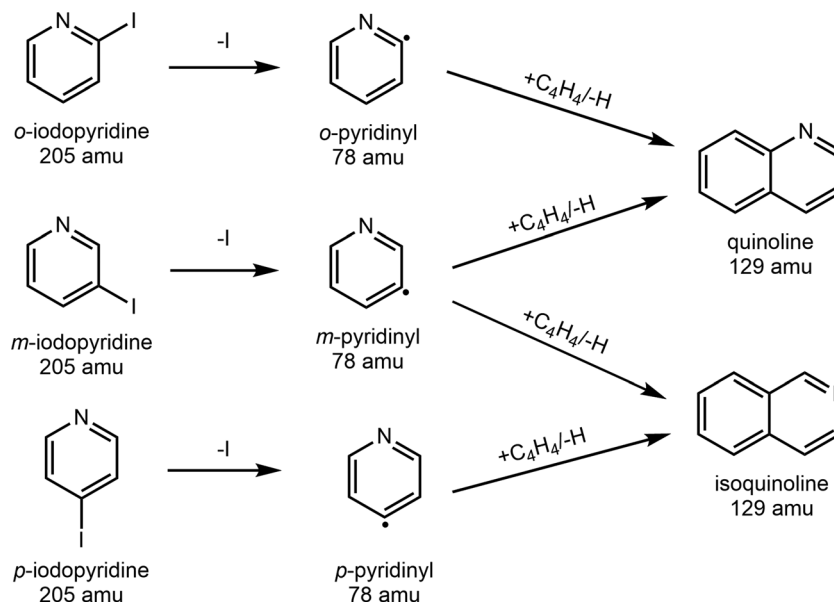


Fig. 1 Schematic representation of the formation of quinoline (C₉H₇N) and isoquinoline (C₉H₇N) from the reaction of *o*-, *m*- and *p*-pyridinyl radicals (C₅H₄N*) with vinylacetylene (C₄H₄). *o*-, *m*- and *p*-pyridinyl radicals are produced from the pyrolysis of corresponding precursors, which are *o*-, *m*- and *p*-iodopyridines (C₅H₄NI), respectively.

and computationally verified framework to PAH formation in extreme environments from low temperature settings to high temperature environments like circumstellar envelopes of carbon rich AGB stars and combustion systems at a few 1000 K.

However, whereas well-defined routes to PAH formation have begun to emerge, surprisingly little is known about the synthesis of their nitrogen-substituted counterparts (NPAHs), which can be derived from PAHs by formally replacing one or more methylidyne (CH) moieties by isoelectronic nitrogen (N) atom(s). Parker *et al.* revealed that the reaction of pyridinyl radicals (*C₅H₄N) – isoelectronic reactants to the phenyl radical (C₆H₅) – with acetylene (C₂H₂) can lead at elevated temperatures to (iso)quinoline (C₉H₇N) *via* the classical Hydrogen Abstraction – Acetylene Addition mechanism in analogy to the formation of naphthalene (C₁₀H₈) *via* HACA.³¹ However, low temperature formation pathways to NPAHs are still obscure. This lack of knowledge is quite remarkable since the 6.2 μm UIR band could also originate from nitrogen-substituted gas phase PAHs.³² Further, considering their molecular structures – PAHs have been contemplated as precursors to biorelevant molecules such as nucleobases – key building blocks in ribonucleic acid (RNA).^{33,34} The astrophysical relevance of nitrogen-substituted aromatic molecules is well documented since the discovery of biorelevant molecules such as vitamin B3 (niacin) and nucleobases (pyrimidines, purines) in carbonaceous chondrites like Murchison.^{35–37} In particular, the detection of terrestrially unusual nucleobases, 6-diaminopurine and 6, 8-diamino-purine in Murchison together with an ¹⁵N/¹⁴N isotope enrichment proposes an extraterrestrial source.^{38,39} Nevertheless, discrete formation mechanisms of NPAHs such as (iso)quinoline are unknown.

Here, we report the results of molecular beam experiments combined with electronic structure calculations on the reaction of three distinct pyridinyl radicals (*ortho*-, *meta*-, *para*-; *o*-, *m*-, *p*-;

*C₅H₄N) with vinylacetylene (H₂CCHCCH; C₄H₄) (Fig. 1). We reveal barrierless formation routes to (iso)quinolines (C₉H₇N) along with their substituted pyridine isomers in analogy to the Hydrogen Abstraction – Vinylacetylene Addition mechanisms leading to naphthalene (C₁₀H₈) in the isoelectronic phenyl – vinylacetylene system.⁴ (Iso)quinoline can be formed *via* a single collision event of the *o*-, *m*- or *p*-pyridinyl radical with vinylacetylene involving a van-der-Waals complex and a submerged barrier in the entrance channel. The facile route to (iso)quinoline in low temperature interstellar and Solar System gas phase environments such as in Saturn’s moon Titan changes our perception how we think about the formation of NPAHs in deep space thus classifying cold molecular clouds like carbon-rich cores of TMC-1 and OMC-1 as potential molecular factories leading to NPAHs in low temperature interstellar environments.

2. Experimental

The experiments were conducted at the Advanced Light Source (ALS) at the Chemical Dynamics Beamline (9.0.2.) exploiting a high-temperature chemical reactor consisting of a resistively-heated silicon carbide (SiC) tube of 20 mm heating length and 1 mm inner diameter.^{2,40,41} This device is situated inside the source chamber of a molecular beam apparatus equipped with a Wiley-McLaren reflectron time-of-flight mass spectrometer (Re-TOF-MS) and designed to study the outcome of elementary chemical reactions leading to PAH growth *in situ* through the reaction of aromatic radicals. In detail, iodinated pyridines (C₅H₄NI) [*o*-iodopyridine (>98%, Sigma-Aldrich); *m*-, and *p*-iodopyridine (>98%, TCI America)] were stored in separate experiments in a stainless-steel bubbler at 293 K. The radical reactants were generated *in situ via* pyrolysis of the iodinated

precursors seeded in vinylacetylene/helium (5% C₄H₄, 95% He; applied gas) carrier gas at a reactor inlet pressure of 300 Torr. The temperature of the SiC tube was determined using a Type-C thermocouple to be 1325 ± 10 K. At this temperature, each iodinated precursor dissociates to the corresponding radical plus atomic iodine *in situ* followed by the reaction of the aromatic radical with vinylacetylene (Fig. 1). The molecular beam passed then through a 2 mm skimmer located 10 mm downstream the reactor and entered the main chamber, which houses the Re-TOF-MS. The products within the supersonic molecular beam were then photoionized in the extraction region of the mass spectrometer by utilizing quasi-continuous tunable synchrotron vacuum ultraviolet (VUV) light. VUV single photon ionization represents essentially a fragment-free ionization technique and is dubbed as a soft ionization method compared to the harsher conditions of electron impact ionization leading often to excessive fragmentation of the parent ion.^{28,42} The ions formed *via* soft photoionization were extracted and introduced onto a microchannel plate detector through an ion lens. Under our experimental condition, the residence time in the reactor tube is few tens to hundreds of μs.⁴³ Control experiments were also conducted by expanding neat helium carrier gas with each iodinated precursor into the resistively-heated silicon carbide tube. No signal at *m/z* = 129 or 130, *i.e.* representing the molecular formula of ionized C₉H₇N and ¹³C₈H₇N, respectively, was observed in these control experiments. Finally, reference PIE curves of helium-seeded C₄H₃-substituted pyridines [2-(but-3-en-1-yn-1-yl)pyridine, (*E*)-2-(but-1-en-3-yn-1-yl)pyridine, 3-(but-3-en-1-yn-1-yl)pyridine, (*E*)-3-(but-1-en-3-yn-1-yl)pyridine, 4-(but-3-en-1-yn-1-yl)pyridine, (*E*)-4-(but-1-en-3-yn-1-yl)pyridine], quinoline (C₉NH₇), and isoquinoline (C₉NH₇) were recorded in the present work within the same experimental setup (ESI⁺). These C₄H₃-branched pyridines were synthesized in house as described in the ESI⁺; quinoline and isoquinoline were purchased from Millipore Sigma (99%+).

3. Theoretical methods

The calculations of the energies and molecular parameters of various intermediates and transition states for the reactions of *o*-, *m*-, and *p*-pyridinyl with vinylacetylene on the C₉NH₉ potential energy surface (PES), as well as of the reactants and possible products were carried out at the G3(MP2,CC)//B3LYP/6-311G(d,p) level of theory. In particular, geometries were optimized and vibrational frequencies were calculated using the density functional B3LYP method^{44,45} with the 6-311G(d,p) basis set. Single-point total energies were subsequently refined *via* a series of coupled clusters CCSD(T) and second-order Møller–Plesset perturbation theory MP2 calculations, with the final energy computed as^{46–48}

$$E[\text{G3(MP2,CC)}] = E[\text{CCSD(T)/6-311G(d,p)}] + E[\text{MP2/G3Large}] - E[\text{MP2/6-311G(d,p)}] + \text{ZPE}[\text{B3LYP/6-311G(d,p)}]$$

The G3(MP2,CC) model chemistry approach normally provides chemical accuracy of 0.01–0.02 Å for bond lengths, 1–2°

for bond angles, and 3–6 kJ mol⁻¹ for relative energies of hydrocarbons, their radicals, reaction energies, and barrier heights in terms of average absolute deviations.⁴⁷ For the entrance van der Waals complexes and ensuing transition states for a covalent bond formation between the C₅NH₄ radicals and C₄H₄, additional single point calculations were carried at the CCSD(T) level with Dunning's correlation-consistent basis sets cc-pVDZ and cc-pVTZ⁴⁹ with subsequent extrapolation to the complete basis set (CBS) limit⁵⁰ and at the explicitly correlated^{51,52} CCSD(T)-F12/cc-pVTZ-f12 level, which also aims to evaluate the CCSD(T)/CBS energy. Geometries and vibrational frequencies of the entrance van der Waals complexes and transition states were recalculated using the doubly-hybrid B2PLYPD3 density functional^{53–55} with the same 6-311G(d,p) basis set. The single-point G3(MP2,CC), CCSD(T)/CBS, and CCSD(T)-F12/cc-pVTZ-f12 calculations were then repeated at the B2PLYPD3/6-311G(d,p)-optimized geometries. These additional calculations were carried out to evaluate the relative energies of the reactant complexes and entrance transition states with respect to the initial reactants, which are critical to determine feasibility of the C₅NH₄ + C₄H₄ reactions at extremely low temperatures. The calculations have shown that relative energies evaluated by the six different methods (B3LYP and B2PLYPD3 for geometries and zero-point vibrational energies (ZPE) and G3(MP2,CC), CCSD(T)/CBS, and CCSD(T)-F12/cc-pVTZ-f12 for single-point energies) agree within ±2 kJ mol⁻¹. The GAUSSIAN 09⁵⁶ and MOLPRO 2010⁵⁷ program packages were employed for the *ab initio* calculations.

Product branching ratios in the C₅NH₄ + C₄H₄ reactions in the limit of zero pressure and extremely low temperature were evaluated through Rice–Ramsperger–Kassel–Marcus (RRKM) calculations^{58–60} of unimolecular rate constants for the reaction steps beginning with the **oi1**, **mi1**, **pi1** intermediates produced in the entrance channels. Here, the rate constants were evaluated as functions of the available internal energy of each intermediate or transition state within the harmonic approximation using B3LYP/6-311G(d,p) frequencies, with the internal energy assumed to be equal to the chemical activation energy, that is, negative of the relative energy of a species with respect to the reactants, which corresponds to a zero collision energy. Only one energy level was considered throughout as at a zero-pressure limit emulating the conditions in cold molecular clouds. RRKM rate constants were used to compute product branching ratios by solving first-order kinetic equations within steady-state approximation.⁶¹

4. Results and discussion

4.1. Experimental results – mass spectrometric result

Once formed in the high-temperature microreactor, the products were probed in a supersonic molecular beam coupled to synchrotron-based mass spectrometry through photoionization. Representative mass spectra recorded at 9.50 eV for the reactions of *o*-, *m*- and *p*-pyridinyl radicals with vinylacetylene along with the data of the control experiments of pyrolyzed,

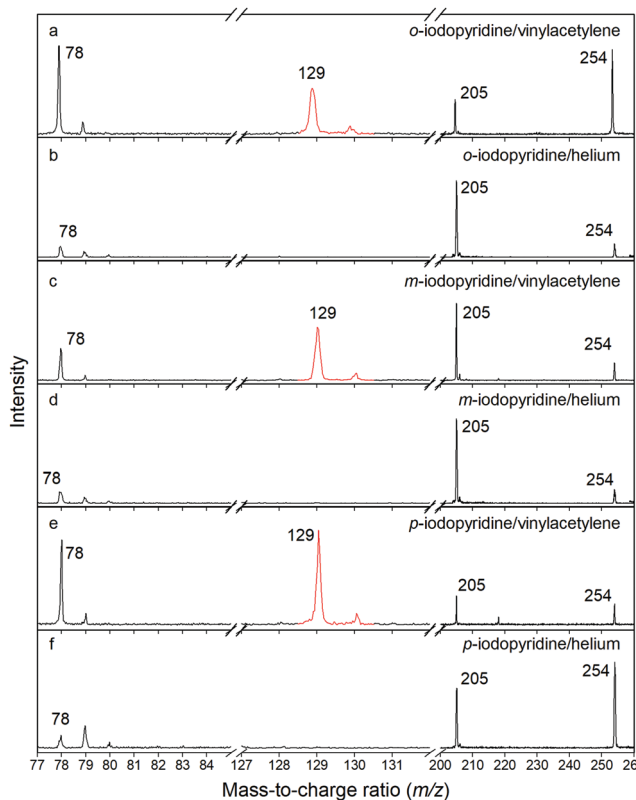


Fig. 2 Comparison of photoionization mass spectra recorded at a photon energy of 9.50 eV. (a) *o*-iodopyridine (C_5H_4NI) – vinylacetylene (C_4H_4) system; (b) *o*-iodopyridine (C_5H_4NI) – helium (He) system; (c) *m*-iodopyridine (C_5H_4NI) – vinylacetylene (C_4H_4) system; (d) *m*-iodopyridine (C_5H_4NI) – helium (He) system; (e) *p*-iodopyridine (C_5H_4NI) – vinylacetylene (C_4H_4) system; and (f) *p*-iodopyridine (C_5H_4NI) – helium (He) system. The mass peaks of the newly formed species of interest along with the ^{13}C -counterparts are highlighted in red.

helium-seeded iodopyridine precursors *without* vinylacetylene are presented in Fig. 2. It is evident that signal at $m/z = 129$ and 130 is *only* observable in the reaction systems (Fig. 2a, c and e) of the pyridinyl radicals with vinylacetylene, but not in the control experiments *without* vinylacetylene (Fig. 2b, d and f). Ion counts at $m/z = 78, 79, 205, 206$ and 254 were detectable in both the reaction systems and in the control experiments; this finding indicates that these species are not formed from reaction of pyridinyl radicals with vinylacetylene. The mass spectra alone deliver compelling evidence that the products at $m/z = 129$ and 130 are the consequence of the reactions of pyridinyl radical (78 amu) with vinylacetylene (52 amu) followed by atomic hydrogen loss. Signal at $m/z = 205$ and 206 can be linked to the precursors (C_5H_4NI) and their ^{13}C -counterparts ($^{13}CC_4H_4NI$). The thermal dissociation of the precursors leads to pyridinyl radicals ($C_5H_4N^\bullet$) observed at $m/z = 78$. Signal at $m/z = 79$ represents a combination of ion counts from ^{13}C -substituted pyridinyl radicals and pyridine (C_5H_5N); the latter is formed *via* hydrogen atom addition to pyridinyl radicals. It is noticeable that iodine (I_2) molecules ($m/z = 254$) are also formed, most likely through recombination of two iodine atoms.

4.2. Experimental Results – Photoionization Efficiency Spectra

Having identified signal at $m/z = 129$ and 130 as the outcome of reactions between pyridinyl radicals with vinylacetylene (Fig. 1 and 2), we are attempting now to identify the nature of the structural isomer(s) formed. This is achieved by extracting the photoionization efficiency curves (PIE); these curves report the ion intensity of a well-defined mass-to-charge ratio as a function of the photon energy. By fitting the experimental PIE curves at well-defined m/z ratios with the linear combination of known, reference PIE curves, we can then identify the molecule(s) contributing to the ion counts at distinct m/z ratios, *i.e.* $m/z = 129$ and 130. Here, the PIE graphs were collected over the photon energy range from 8.00 to 10.00 eV in steps of 0.05 eV (Fig. 3). It is important to note that the experimental PIE profiles of $m/z = 129$ and 130 are superimposable after rescaling for each system; this indicates that signal at $m/z = 130$ is associated with the ^{13}C -counterparts of $m/z = 129$ ($C_9H_7N^+$). In detail, a linear combination of recorded reference PIE curves of distinct C_9H_7N isomers could replicate the experimental PIE curves for each system (Fig. 3).

First, in the *o*-pyridinyl – vinylacetylene system, the PIE curve of $m/z = 129$ reveals a clear onset at 8.45 ± 0.05 eV (Fig. 3a); this onset corresponds to the adiabatic ionization energy (IE) of (*E*)-2-(but-1-en-3-yn-1-yl)pyridine (8.45 ± 0.05 eV; **P3**) (Fig. 4). However, this isomer cannot alone replicate the experimentally recorded PIE curve. The overall fit reveals that a linear combination of the PIE curves of quinoline (**P1**), (*E*)-2-(but-1-en-3-yn-1-yl)pyridine (**P3**), and 2-(but-3-en-1-yn-1-yl)pyridine (**P4**), could replicate the experimental data. The ion counts of the three isomers have a branching ratio of **P1** : **P3** : **P4** of $19.6 \pm 2.0\%$: $70.3 \pm 7.0\%$: $10.1 \pm 1.0\%$ at the photon energy of 10.00 eV. It should be noticed that these percentage values do not represent the branching ratios of the individual isomer; the latter cannot be determined since their photoionization cross sections are unknown and hence not available. Second, in the *m*-pyridinyl – vinylacetylene system (Fig. 3c and d), the onset at 8.50 ± 0.05 eV corresponds to the IE of (*E*)-3-(but-1-en-3-yn-1-yl)pyridine (8.50 ± 0.05 eV; **P5**). The overall fit could be achieved with a combination of four reference C_9H_7N PIE curves: quinoline (**P1**), isoquinoline (**P2**), (*E*)-3-(but-1-en-3-yn-1-yl)pyridine (**P5**), and 3-(but-3-en-1-yn-1-yl)pyridine (**P6**). The branching ratio of the ion counts of these four isomers **P1** : **P2** : **P5** : **P6** was determined to be $7.8 \pm 0.8\%$: $7.9 \pm 0.8\%$: $75.8 \pm 7.6\%$: $2.5 \pm 0.3\%$ at 10.00 eV. Finally, in the *p*-pyridinyl – vinylacetylene system (Fig. 3e and f), the onset agrees with the adiabatic IE of isoquinoline (8.55 ± 0.05 eV; **P2**). The measured PIE curve at $m/z = 129$ could be fit with isoquinoline (**P2**), (*E*)-4-(but-1-en-3-yn-1-yl)pyridine (**P7**), and 4-(but-3-en-1-yn-1-yl)pyridine (**P8**) with ratios of the ion counts for **P2** : **P7** : **P8** of $23.7 \pm 2.4\%$: $66.1 \pm 6.7\%$: $10.2 \pm 1.0\%$ at 10.00 eV.

Overall, the reactions of *o*-, *m*- and *p*-pyridinyl with vinylacetylene reveal the formation of bicyclic reaction products (quinoline, isoquinoline) along with but-3-en-1-yn-1-yl- and (*E*)-but-1-en-3-yn-1-yl-substituted pyridines at the *o*-, *m*- and *p*-positions, respectively (Fig. 4).

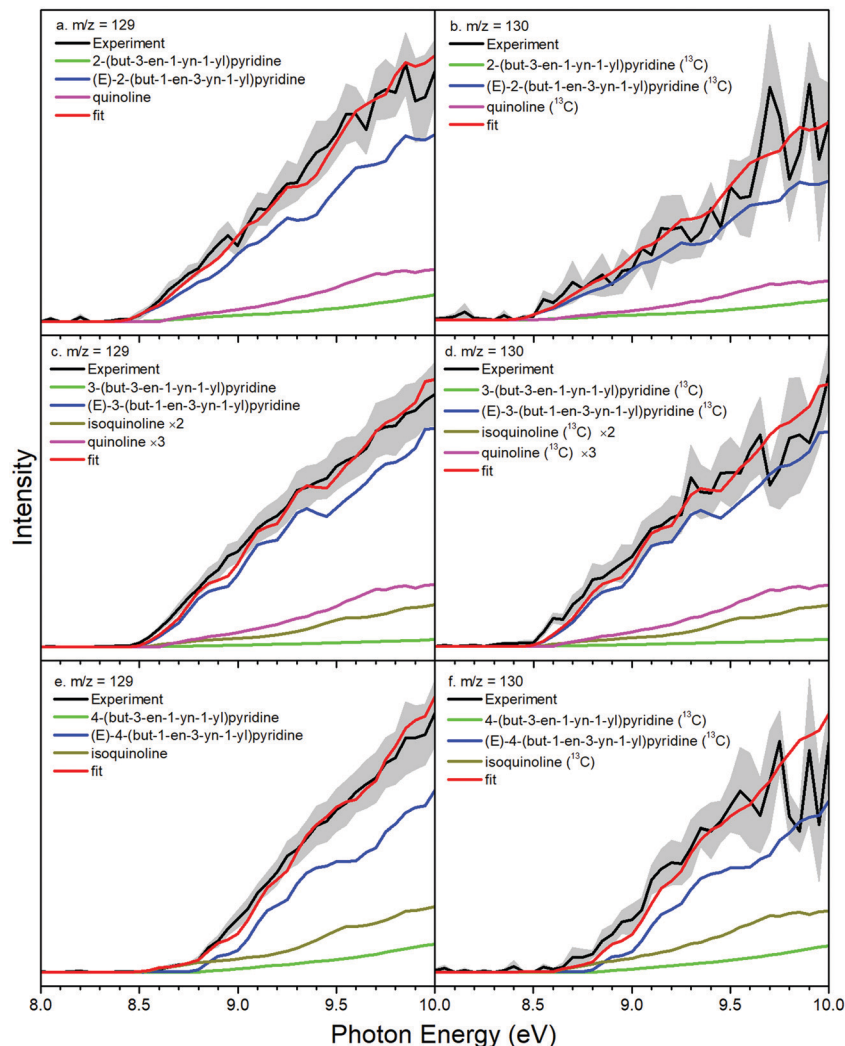


Fig. 3 Photoionization efficiency (PIE) curves of $m/z = 129$ and 130 for reactions *o*-pyridinyl – vinylacetylene (a and b), *m*-pyridinyl – vinylacetylene (c and d), and *p*-pyridinyl/vinylacetylene (e and f). Black: experimentally derived PIE curves; colored lines (green, blue, dark yellow and purple): reference PIE curves; red lines: overall fit. The overall error bars consist of two parts: $\pm 10\%$ based on the accuracy of the photodiode and a 1σ error of the PIE curve averaged over the individual scans.

Quinoline is formed in the *o*- and *m*-pyridinyl – vinylacetylene systems, while isoquinoline is detected in the *m*- and *p*-pyridinyl – vinylacetylene systems. The reference PIE curves for both quinoline and isoquinoline are different both in the onset of photoionization signal (ionization energy) and their shapes (Fig. S4, ESI[†]).

4.3 Theoretical results

We are now merging the experimental results with electronic structure calculations in an attempt to unravel the reaction mechanisms. PES profiles for the reactions of pyridinyl radicals with vinylacetylene, where the latter adds to the radical site by its vinylic end, operational even at very low temperatures are exhibited in Fig. 5a–c for *o*-, *m*-, and *p*-pyridinyl, respectively. The surfaces corresponding to C_4H_4 addition by the C_2H group are provided in the ESI[†] (Fig. S5).

4.3.1 *o*-Pyridinyl - vinylacetylene system. Let us first focus on the reaction mechanism in the *o*-pyridinyl - vinylacetylene

system (Fig. 5a and Fig. S5a, ESI[†]). The vinylacetylene molecule approaches the *o*-pyridinyl radical forming a weakly stabilized (-10 kJ mol^{-1}) van der Waals complex **oi0**. This complex isomerizes *via* addition of the radical center of the *o*-pyridinyl radical to the CH_2 moiety of the vinylacetylene molecule forming a nitrogen-containing resonantly stabilized doublet radical intermediate **oi1**. As computed at the G3(MP2,CC)//B3LYP/6-311G(d,p)+ZPE level of theory, this addition requires overcoming a barrier of 9 kJ mol^{-1} meaning that the energy of the transition state is 1 kJ mol^{-1} below the total energy of the separated reactants, hence, a submerged barrier. At the CCSD(T)/CBS and CCSD(T)-F12/cc-pVTZ-f12 levels of theory, the position of the transition state is close to $+1 \text{ kJ mol}^{-1}$, which indicates that, considering the anticipated error bars of the calculations, the addition proceeds either without or with a very low activation energy. The intermediate **oi1** can decompose *via* atomic hydrogen loss to (*E*)-2-(but-1-en-3-yn-1-yl)pyridine (**P3**). Alternatively, an isomerization sequence *via* a hydrogen shift

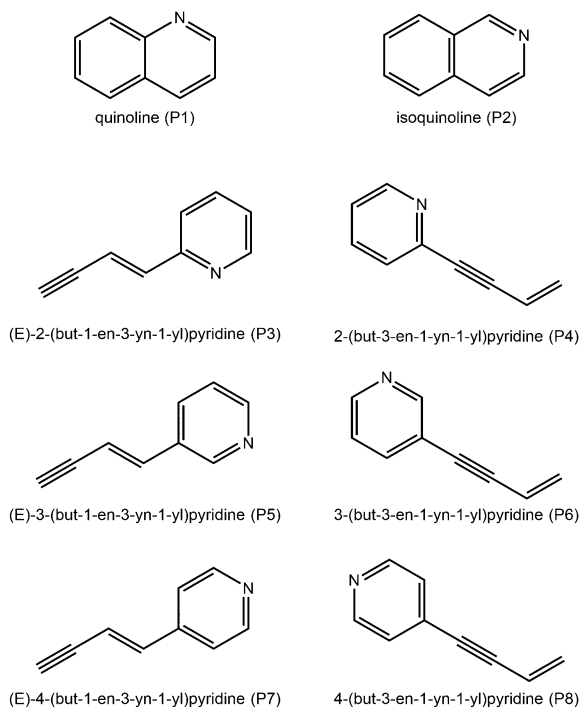


Fig. 4 The molecular structures of the products observed in this work.

from the aromatic ring to the C2 atom of the chain moiety (**oi2**), cyclization (**oi3**), and a hydrogen shift to the carbene moiety to **oi4** is terminated by an atomic hydrogen loss followed by aromatization to form the bicyclic quinoline (**P1**). It should be noted that, besides the entrance transition state whose relative energy could be slightly positive but close to zero, all intermediates and transition states of this reaction sequence are located below the energy of the separated reactants; therefore, the reactions to form **P1** and **P3** are actually barrierless or nearly barrierless.

Apart from these two products observed in *o*-pyridinyl – vinylacetylene system, a third product 2-(but-3-en-1-yn-1-yl)pyridine (**P4**) was also detected. The PES (Fig. S5a, ESI[†]) indicates that the van-der Waals structure **oi0** can isomerize *via* addition of the *o*-pyridinyl to the terminal CH moiety of vinylacetylene yielding intermediate **oi5**; the transition state involved is higher than the energy of the separated reactants. A hydrogen atom loss from the acetylenic group of the vinylacetylene chain leads to the formation of 2-(but-3-en-1-yn-1-yl)pyridine (**P4**) in an overall exoergic reaction (-11 kJ mol^{-1}). However, the exit transition state resides 8 kJ mol^{-1} above the separated products. This barrier can be easily overcome in the high temperature conditions of the reactor, but it cannot be passed in cold environments such as in molecular clouds (10 K).

Alternatively, **oi5** can isomerize to **oi7** *via* hydrogen atom migration from the aromatic ring to the C2 atom of the side chain. Successive hydrogen migrations drive **oi7** to **oi8** and **oi9**, from C1 in the sidechain back to C3 on the ring and from C4 to C1 at the C_4H_4 moiety, respectively. Hydrogen atom loss from **oi9** yields the product (*E*)-2-(but-1-en-3-yn-1-yl)pyridine (**P3**).

In an alternative pathway, **oi9** isomerizes to an exotic bicyclic structure with a six and a four-membered-ring intermediate **oi10**, which then ring-opens to **oi11** thus achieving a conformational change from *trans* in **oi9** to *cis* in **oi11**; the latter isomerizes through ring-closure to **oi12**, which contains the quinoline backbone. This intermediate eventually loses a hydrogen atom to yield quinoline (**P1**). Alternatively, starting from **oi7**, a cyclization process leads to the formation of **oi13**, which then ring opens to **oi14**; here again, the four-member ring closure and opening change the conformation of the side chain from *trans* in **oi7** to *cis* in **oi14**. Intermediate **oi15** – produced *via* the ring-closure of **oi14** – can eject atomic hydrogen to form quinoline (**P1**). Finally, hydrogen shifts dictate the sequence from **oi14** to **oi16**, which *cis*–*trans* isomerizes to **oi17**. Hydrogen atom losses convert **oi16** and **oi17** to (*Z*)-2-(but-1-en-3-yn-1-yl)pyridine (**P9**) and (*E*)-2-(but-1-en-3-yn-1-yl)pyridine (**P3**), respectively.

4.3.2 *m*-Pyridinyl – vinylacetylene system. Similar to the mechanisms in the *o*-pyridinyl – vinylacetylene system, the vinylacetylene molecule approaches the *m*-pyridinyl radical forming a weakly stabilized (-8 kJ mol^{-1}) van der Waals complex **mi0** (Fig. 5b and Fig. S5b, ESI[†]). The complex isomerizes to intermediate **mi1** *via* addition of the radical center in *m*-pyridinyl to the CH_2 moiety of vinylacetylene through a small barrier of 5 kJ mol^{-1} . Once again, the barrier to addition is below the energy of the separated reactants and hence can be classified as a submerged barrier. Moreover, in this case CCSD(T)/CBS and CCSD(T)-F12 levels of theory confirm that the energy of the transition state is negative relative to the reactants. A hydrogen atom loss from **mi1** leads to the experimentally detected product (*E*)-3-(but-1-en-3-yn-1-yl)pyridine (**P5**). Alternatively, the reaction sequence **mi1** → **mi2** → **mi3** → **mi4** → **P1** involving a hydrogen shift from the aromatic ring to the C2 atom in the chain, cyclization, a hydrogen migration in the aromatic moiety to the carbene, and hydrogen atom elimination leading eventually to the formation of quinoline (**P1**). A second pathway *via* **mi1** → **mi5** → **mi6** → **mi7** → **P2**, effectively converts **mi1** to isoquinoline (**P2**) along with a hydrogen atom. All barriers involved in these reaction pathways are below the separated reactants. Note that from **mi1**, quinoline formation is suggested to proceed favorable compared to isoquinoline considering the lower barriers for hydrogen migrations (to **mi2** *versus* **mi5**) and ring closure (to **mi3** *versus* **mi6**).

Besides quinoline (**P1**), isoquinoline (**P2**) and (*E*)-3-(but-1-en-3-yn-1-yl)pyridine (**P5**), 3-(but-3-en-1-yn-1-yl)pyridine (**P6**) is also a detected product in the *m*-pyridinyl – vinylacetylene experiment. As we will demonstrate below, pathways to this product require overcoming transition states located above the energy of the separated reactants. In detail, **P6** can be formed *via* hydrogen atom loss from intermediate **mi8**, which is generated *via* isomerization of **mi0** through the addition of the radical center in *m*-pyridinyl to the terminal acetylenic moiety of C_4H_4 molecule. This reaction pathway requires overcoming a barrier of only 3 kJ mol^{-1} higher than the separated reactants; this process can happen under the high-temperature condition in

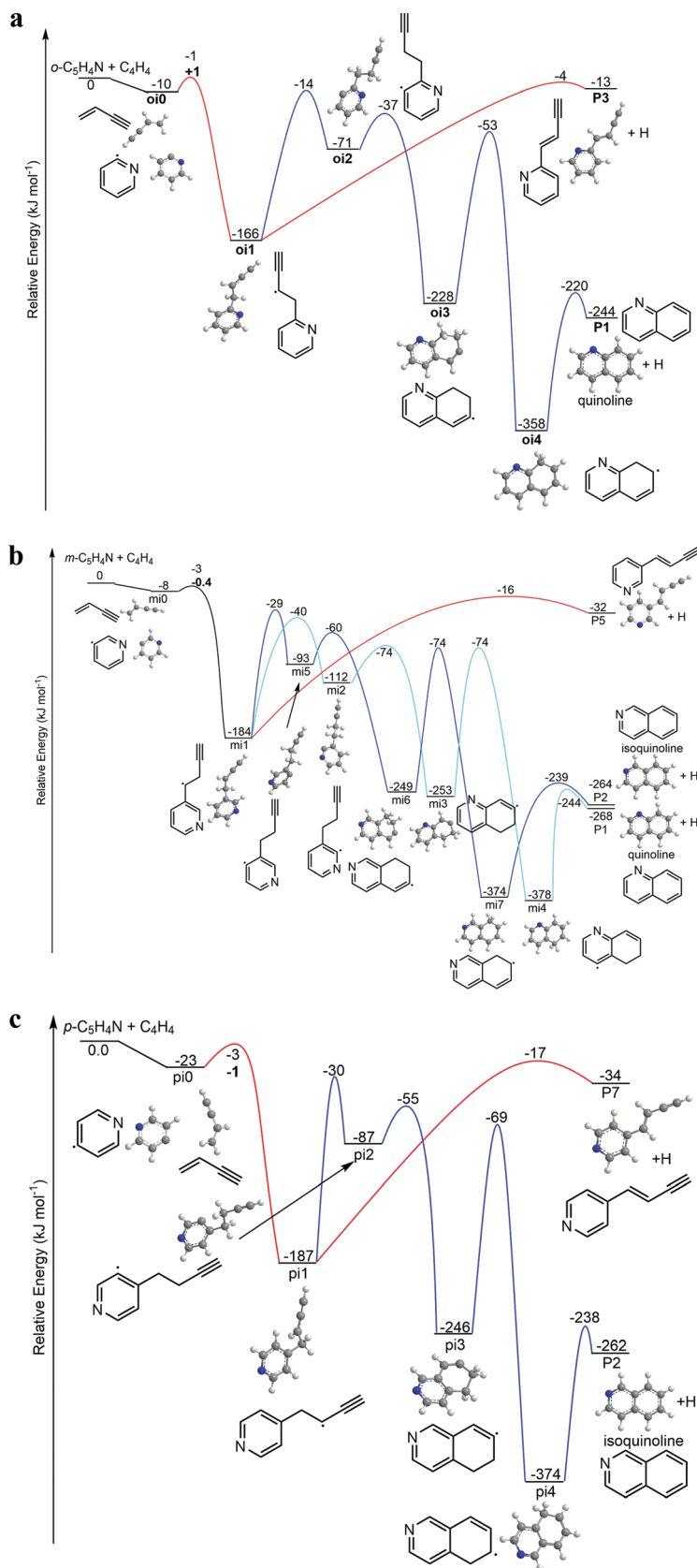


Fig. 5 (a) Computed potential energy surface (PES) for the reaction system of *o*-pyridinyl ($\text{C}_5\text{H}_4\text{N}^*$) and vinylacetylene (C_4H_4). The energies calculated at the G3(MP2,CC)//B3LYP/6-311G(d,p)+ZPE level of theory are presented in units of kJ mol^{-1} . The bold number shows the relative energy of the **oi0–oi1** transition state calculated at the CCSD(T)-F12/cc-pVTZ-f12//B3LYP/6-311G(d,p)+ZPE level. Only pathways open under conditions in cold molecular

clouds are shown. For a surface describing the addition by the acetylenic end of C_4H_4 , please confer to Fig. S5a (ESI[†]). (b) Computed PES for the reaction system of *m*-pyridinyl ($C_5H_4N^*$) and vinylacetylene (C_4H_4). The energies calculated at the G3(MP2,CC)//B3LYP/6-311G(d,p) + ZPE level of theory are presented in units of kJ mol^{-1} . The bold number shows the relative energy of the **mi0–mi1** transition state calculated at the CCSD(T)-F12/cc-pVTZ-f12//B3LYP/6-311G(d,p)+ZPE level. Only pathways open under conditions in cold molecular clouds are shown. For a surface describing the addition by the acetylenic end of C_4H_4 , please confer to Fig. S5b (ESI[†]). (c) Computed PES for the reaction system of *p*-pyridinyl ($C_5H_4N^*$) and vinylacetylene (C_4H_4). The energies calculated at the G3(MP2,CC)//B3LYP/6-311G(d,p)+ZPE level of theory are presented in units of kJ mol^{-1} . The bold number shows the relative energy of the **pi0–pi1** transition state calculated at the CCSD(T)-F12/cc-pVTZ-f12//B3LYP/6-311G(d,p)+ZPE level. Only pathways open under conditions in cold molecular clouds are shown. For a surface describing the addition by the acetylenic end of C_4H_4 , please confer to Fig. S5c (ESI[†]).

our experiments, but not in cold molecular clouds. Intermediate **mi8** may also undergo isomerization to **mi10** and/or **mi17** *via* distinct hydrogen shifts. These intermediates eventually yield through multi-step isomerization pathways to quinoline (**P1**), isoquinoline (**P2**), (*E*)-3-(but-1-en-3-yn-1-yl)pyridine (**P5**), (*Z*)-3-(but-1-en-3-yn-1-yl)pyridine (**P10**), and 3-(but-3-en-1-yn-1-yl)pyridine (**P6**). Finally, **mi9** is generated *via* addition of the *m*-pyridinyl radical to the CH vinylenic carbon atom of vinylacetylene by overcoming a barrier of 13 kJ mol^{-1} relative to the reactants. The subsequent reaction sequences may lead to quinoline (**P1**), isoquinoline (**P2**), and (*E*)-3-(but-1-en-3-yn-1-yl)pyridine (**P5**). Overall, unlike the sole detection and formation of the NPAH quinoline in the *o*-pyridinyl – vinylacetylene system, two NPAHs (quinoline, isoquinoline) are formed in the *m*-pyridinyl system since **mi1** can undergo hydrogen migration from the ortho and para carbon atom of the pyridine moiety to the C2 carbon of the vinylacetylene chain.

4.3.3 *p*-Pyridinyl – vinylacetylene system. As presented in Fig. 5c, the PES for the *p*-pyridinyl – vinylacetylene reaction system for the C_4H_4 addition by its vinylic end has similar features of the *o*-pyridinyl – vinylacetylene system leading eventually to the formation of isoquinoline (**P2**) and (*E*)-4-(but-1-en-3-yn-1-yl)pyridine (**P7**). The key difference between these two systems is that the addition *via* the submerged barrier leads eventually to the formation of isoquinoline (**P2**) instead of quinoline (**P1**), owing to the discrepancy between the location of the radical centers in the *ortho*- and *para*-positions of pyridinyl radicals. It should be also noted that the CCSD(T)/CBS and CCSD(T)-F12 calculations for the *p*-pyridinyl plus vinylacetylene system corroborate negative energy of the entrance transition state with respect to the reactants and hence a submerged character of the reaction barrier. The third experimentally observed product 4-(but-3-en-1-yn-1-yl)pyridine (**P8**) is formed in analogy to 2-(but-3-en-1-yn-1-yl)pyridine (**P4**) and 3-(but-3-en-1-yn-1-yl)pyridine (**P6**) *via* hydrogen atom loss of intermediate **pi6**; this intermediate is generated from the isomerization of the van-der Waals complex **pi0** *via* addition of *p*-pyridinyl to the CH group of vinylacetylene. High energy pathways have to overcome barriers, which are not accessible in cold molecular clouds (Fig. S5c, ESI[†]).

5. Conclusions

Our study provides compelling evidence on the de-facto barrierless formation of two NPAHs isovalent to naphthalene ($C_{10}H_8$) – quinoline (C_9H_7N , **P1**) and isoquinoline (C_9H_7N , **P2**) – in cold

molecular clouds in overall exoergic reactions. In all three systems, the reactions are initiated by the formation of a van der Waals complex (**oi0**, **mi0**, **pi0**) stabilized by 8 to 23 kJ mol^{-1} with respect to the separated reactants. These complexes then isomerize *via* addition of the carbon-centered radicals to the CH_2 moiety of vinylacetylene *via* barriers lower than the energy of the separated reactants (submerged barriers) leading to resonantly stabilized doublet radical intermediates (**oi1**, **mi1**, **pi1**). While a submerged character of the entrance transition states is consistently confirmed by different levels of theoretical calculations in the *m*- and *p*-pyridinyl – vinylacetylene reaction systems, for *o*-pyridinyl the barrier might be slightly positive, but it is close to zero within the expected error bars of the present calculations. Each of the initially formed radical intermediates can evolve through essentially two reaction pathways. Pathway one is dictated by a hydrogen atom loss from the CH_2 moiety of vinylacetylene leading in weakly exoergic reactions (-13 to -34 kJ mol^{-1}) to *o*-, *m*-, and *p*- C_4H_3 substituted pyridines: 2-, 3-, and 4-(but-1-en-3-yn-1-yl)pyridines (**P3**, **P5**, **P7**). Alternatively, **oi1**, **mi1**, **pi1** eventually form quinoline (C_9H_7N , **P1**) and isoquinoline (C_9H_7N , **P2**) *via* three isomerization steps through hydrogen shifts from the pyridine moiety to the C2 atom of the side chain, cyclization, hydrogen shift in the annulated ring moiety to the carbene carbon atom terminated by hydrogen atom loss and aromatization in overall exoergic reactions. These pathways follow identical features as the Hydrogen Abstraction – Vinylacetylene Addition mechanism^{2,4,5,8} leading to the iso-valent naphthalene ($C_{10}H_8$) molecule through barrierless ring annulation of the phenyl radical – the isoelectronic species of *o*-, *m*-, and *p*-pyridinyl). Comparing the pathways of both NPAHs to PAH formation, the replacement of the CH moiety in the phenyl reactant by a nitrogen atom effectively destabilizes the reaction intermediates and transition states on the inherent PESs by about 20 kJ mol^{-1} . However, the apparent facile concept of isoelectronicity, which predicts analogous reaction pathways to naphthalene and (iso)quinoline based on the $C_6H_5-C_4H_4$ and $C_5H_4N-C_4H_4$ and hence the replacement of a CH moiety by a nitrogen atom in the aromatic reactant cannot be expanded to the vinylacetylene reactant. The replacement of a CH moiety by a nitrogen leads to vinyl cyanide (C_2H_3CN). The isovalent $C_6H_5-C_2H_3CN$ system was shown not to form (iso)quinoline under conditions of cold molecular clouds. Here, in strong discrepancy to the $C_5H_4N-C_4H_4$ systems, the nitrogen atom does not act as a spectator, but is actively engaged in the chemistry in the $C_6H_5-C_2H_3CN$ system through the formation of a carbon–hydrogen bond. The involvement of the nitrogen atom in the reaction dynamics and the stability of the cyano group results

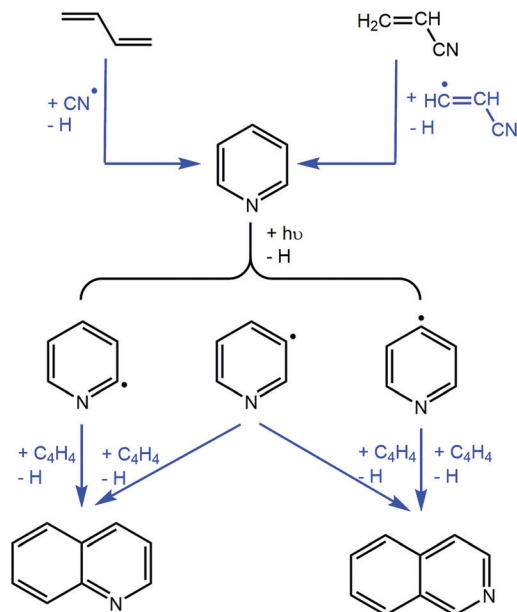


Fig. 6 Potential pathways leading to the formation of pyridine and subsequently to (iso)quinoline through various mechanisms under low-temperature conditions.

in energetically unfavorable transition states located at least 13 kJmol^{-1} above the separated reactants thus effectively blocking this pathway in cold molecular clouds, and also in the experiments.⁶² Based on the PESs relevant to conditions in cold molecular clouds (Fig. 5a–c), we also conducted statistical calculations to predict the relative branching ratios of the (but-1-en-3-yn-1-yl)pyridines *versus* the NPAHs (quinoline, isoquinoline). At the zero-pressure and zero-temperature limit, the RRKM calculations reveal overwhelming formation of the NPAHs: 99.7% of quinoline to 0.3% of **P3** for *o*-pyridinyl plus C₄H₄, 98.9% of isoquinoline to 1.1% of **P7** for *p*-pyridinyl, and 94.4% of quinoline and 5.5% of isoquinoline to 0.1% of **P5** for *m*-pyridinyl. However, higher temperatures increase the relative yields of the (but-1-en-3-yn-1-yl)pyridines **P1**, **P3**, and **P5** due to entropic preference of their formation channels.

Note that besides the aforementioned products, the present studies also identified three (but-3-en-1-yn-1-yl) pyridine products (**P4**, **P6**, **P8**), which can be formally derived by replacing the terminal carbon atom of the acetylenic functional group in vinylacetylene by distinct pyridinyl groups. In molecular clouds, however, pathways to these isomers are blocked since that the addition of the pyridinyl radicals to the terminal carbon atom of the acetylenic moiety has entrance barriers above the energy of the separated reactants (Fig. S5a–c, ESI†). However, these barriers can be overcome under the high temperature conditions in our chemical reactor.

To summarize, the present work provides a facile conceptual framework on the barrierless, low temperature formation of two prototypes of NPAHs – quinoline (C₉H₇N, **P1**) and isoquinoline (C₉H₇N, **P2**) – in the gas phase of cold molecular clouds in analogy to the Hydrogen Abstraction – Vinylacetylene Addition mechanism.^{2,4,5,8} Low temperature conditions also hold for

hydrocarbon-rich atmospheres of planets, their moons (Titan),⁶³ and *trans*-Neptunian Objects (TNOs) such as Pluto,⁶⁴ where solar photons initiate a vigorous low temperature photochemistry of their methane–nitrogen based atmospheres. The pathways derived here require the presence of pyridine (C₅H₅N), which can be photolyzed to *o*-, *m*-, and *p*-pyridinyl radicals (C₅H₄N), and vinylacetylene (C₄H₄), which was recently observed in the cold molecular cloud TMC-1,⁶⁵ but not (yet) in Titan's or Pluto's atmosphere (Fig. 6). However, both in the interstellar medium and in Pluto's and Titan's atmospheres, the ethylene (C₂H₄) and ethynyl (C₂H) reactants can easily form vinylacetylene as demonstrated by Zhang *et al.*⁶⁶ Three barrierless and exoergic pathways have been derived to form pyridine: (i) reaction of 1,3-butadiene (C₄H₆) with cyano (CN) radicals (albeit with yields of a fraction of a percent at most),^{67,68} (ii) reaction of vinylcyanide (C₂H₃CN) with cyano vinyl (HCCHCN),³¹ and (iii) reactions of methylidyne (CH) radicals with pyrrole (C₄H₅N).⁶⁹ Therefore, the aforementioned 'ingredients' – with the exception of pyrrole – suggest that pyridine, quinoline, and isoquinoline should form in cold molecular clouds as well as in Titan's and Pluto's atmosphere. However, the detectability of (iso)quinoline by microwave spectroscopy on these environments critically depends on the actual fractional abundance, which are dictated not only by their formation, but also destruction pathways such as by photodissociation^{70–72} and fast chemical reactions such as with ground state carbon atoms.⁷³

Author contributions

R. I. K. directed the overall project. A. H. H. synthesized the molecular calibration chemicals; L. Z., M. P., B. X. and W. L. carried out the experimental measurements; L. Z. performed the data analysis; A. S. K., M. M. E., E. K. B. V. N. A. and A. M. M. carried out the theoretical analysis; ALL the authors discussed the data. R. I. K., M. A. and A. M. M. supervised the project. S. F. W. supervised the synthesis processes. L. Z., R. I. K. and A. M. M. wrote the manuscript.

Conflicts of interest

The authors declare no competing financial interests.

Acknowledgements

This work was supported by the US Department of Energy, Basic Energy Sciences DE-FG02-03ER15411 (experimental studies) and DE-FG02-04ER15570 (computational studies), to the University of Hawaii and to Florida International University. M. A. and W. L. are supported by the Director, Office of Science, Office of Basic Energy Sciences, of the U.S. Department of Energy under Contract No. DE-AC02-05CH11231, through the Gas Phase Chemical Physics Program, Chemical Sciences Division. The Advanced Light Source is supported by the same contract. Theoretical calculations at Lebedev Physics Institute were supported by the Ministry of Higher Education and Science of the Russian Federation by the grant no. 075-15-2021-597.

References

- 1 L. Zhao, R. I. Kaiser, W. Lu, B. Xu, M. Ahmed, A. N. Morozov, A. M. Mebel, A. H. Howlader and S. F. Wnuk, *Nat. Commun.*, 2019, **10**, 3689.
- 2 L. Zhao, R. I. Kaiser, B. Xu, U. Ablikim, M. Ahmed, M. M. Evseev, E. K. Bashkirov, V. N. Azyazov and A. M. Mebel, *Nat. Astron.*, 2018, **2**, 973–979.
- 3 L. Zhao, R. I. Kaiser, B. Xu, U. Ablikim, M. Ahmed, D. Joshi, G. Veber, F. R. Fischer and A. M. Mebel, *Nat. Astron.*, 2018, **2**, 413–419.
- 4 L. Zhao, R. I. Kaiser, B. Xu, U. Ablikim, M. Ahmed, M. V. Zagidullin, V. N. Azyazov, A. H. Howlader, S. F. Wnuk and A. M. Mebel, *J. Phys. Chem. Lett.*, 2018, **9**, 2620–2626.
- 5 L. Zhao, R. I. Kaiser, B. Xu, U. Ablikim, W. Lu, M. Ahmed, M. M. Evseev, E. K. Bashkirov, V. N. Azyazov, M. V. Zagidullin, A. N. Morozov, A. H. Howlader, S. F. Wnuk, A. M. Mebel, D. Joshi, G. Veber and F. R. Fischer, *Nat. Commun.*, 2019, **10**, 1510.
- 6 L. Zhao, M. Prendergast, R. I. Kaiser, B. Xu, U. Ablikim, W. Lu, M. Ahmed, A. D. Oleinikov, V. N. Azyazov and A. H. Howlader, *Phys. Chem. Chem. Phys.*, 2019, **21**, 16737–16750.
- 7 L. Zhao, M. B. Prendergast, R. I. Kaiser, B. Xu, U. Ablikim, M. Ahmed, B. J. Sun, Y. L. Chen, A. H. Chang and R. K. Mohamed, *Angew. Chem., Int. Ed.*, 2019, **58**, 17442–17450.
- 8 L. Zhao, B. Xu, U. Ablikim, W. Lu, M. Ahmed, M. M. Evseev, E. K. Bashkirov, V. N. Azyazov, A. H. Howlader and S. F. Wnuk, *Chem. Phys. Chem.*, 2019, **20**, 791–797.
- 9 L. Zhao, S. Doddipatla, R. I. Kaiser, W. Lu, O. Kostko, M. Ahmed, L. B. Tuli, A. N. Morozov, A. H. Howlader and S. F. Wnuk, *Phys. Chem. Chem. Phys.*, 2021, **23**, 5740–5749.
- 10 D. S. Parker, R. I. Kaiser, T. P. Troy and M. Ahmed, *Angew. Chem., Int. Ed.*, 2014, **53**, 7740–7744.
- 11 M. Baroncelli, Q. Mao, S. Galle, N. Hansen and H. Pitsch, *Phys. Chem. Chem. Phys.*, 2020, **22**, 4699–4714.
- 12 D. S. Parker, F. Zhang, Y. S. Kim, R. I. Kaiser, A. Landera, V. V. Kislov, A. M. Mebel and A. Tielens, *Proc. Natl. Acad. Sci. U. S. A.*, 2012, **109**, 53–58.
- 13 D. D. S. Parker, D. F. Zhang, D. R. I. Kaiser, D. V. V. Kislov and D. A. M. Mebel, *Chem. – Asian J.*, 2011, **6**, 3035–3047.
- 14 R. I. Kaiser and N. Hansen, *J. Phys. Chem. A*, 2021, **125**, 3826–3840.
- 15 P. Ehrenfreund and M. A. Sephton, *Faraday Discuss.*, 2006, **133**, 277–288.
- 16 E. Herbst and E. F. van Dishoeck, *Annu. Rev. Astron. Astrophys.*, 2009, **47**, 427–480.
- 17 W. W. Duley, *Astrophys. J.*, 2000, **528**, 841–848.
- 18 A. M. Ricks, G. E. Douberly and M. A. Duncan, *Astrophys. J.*, 2009, **702**, 301–306.
- 19 A. G. G. M. Tielens, *Annu. Rev. Astron. Astrophys.*, 2008, **46**, 289–337.
- 20 J. Puget and A. Léger, *Annu. Rev. Astron. Astrophys.*, 1989, **27**, 161–198.
- 21 R. Zenobi, J. M. Philippoz, R. N. Zare, M. R. Wing, J. L. Bada and K. Marti, *Geochim. Cosmochim. Acta*, 1992, **56**, 2899–2905.
- 22 H. Naraoka, A. Shimoyama and K. Harada, *Mineral. Mag.*, 1998, **62A**, 1056–1057.
- 23 H. Naraoka, A. Shimoyama and K. Harada, *Earth Planet. Sci. Lett.*, 2000, **184**, 1–7.
- 24 A. M. Mebel, A. Landera and R. I. Kaiser, *J. Phys. Chem. A*, 2017, **121**, 901–926.
- 25 C. He, A. A. Nikolayev, L. Zhao, A. M. Thomas, S. Doddipatla, G. R. Galimova, V. N. Azyazov, A. M. Mebel and R. I. Kaiser, *J. Phys. Chem. A*, 2021, **125**, 126–138.
- 26 N. Hansen, M. Schenk, K. Moshhammer and K. Kohse-Höinghaus, *Combust. Flame*, 2017, **180**, 250–261.
- 27 K. Johansson, M. Head-Gordon, P. Schrader, K. Wilson and H. Michelsen, *Science*, 2018, **361**, 997–1000.
- 28 H. Jin, L. Xing, D. Liu, J. Hao, J. Yang and A. Farooq, *Combust. Flame*, 2021, **225**, 524–534.
- 29 J. D. Savee, T. M. Selby, O. Welz, C. A. Taatjes and D. L. Osborn, *J. Phys. Chem. Lett.*, 2015, **6**, 4153–4158.
- 30 P. Liu, H. Jin, B. Chen, J. Yang, Z. Li, A. Bennett, A. Farooq, S. M. Sarathy and W. L. Roberts, *Fuel*, 2021, **295**, 120580.
- 31 D. S. N. Parker, R. I. Kaiser, O. Kostko, T. P. Troy, M. Ahmed, B.-J. Sun, S.-H. Chen and A. H. H. Chang, *Phys. Chem. Chem. Phys.*, 2015, **17**, 32000–32008.
- 32 D. M. Hudgins, C. W. Bauschlicher Jr and L. J. Allamandola, *Astrophys. J.*, 2005, **632**, 316.
- 33 Z. Peeters, O. Botta, S. B. Charnley, R. Ruiterkamp and P. Ehrenfreund, *Astrophys. J.*, 2003, **593**, L129–L132.
- 34 M. P. Kroonblawd, R. K. Lindsey and N. Goldman, *Chem. Sci.*, 2019, **10**, 6091–6098.
- 35 K. E. Smith, M. P. Callahan, P. A. Gerakines, J. P. Dworkin and C. H. House, *Geochim. Cosmochim. Acta*, 2014, **136**, 1–12.
- 36 M. P. Callahan, K. E. Smith, H. J. Cleaves, J. Ruzicka, J. C. Stern, D. P. Glavin, C. H. House and J. P. Dworkin, *Proc. Natl. Acad. Sci. U. S. A.*, 2011, **108**, 13995–13998.
- 37 Z. Martins, O. Botta, M. L. Fogel, M. A. Sephton, D. P. Glavin, J. S. Watson, J. P. Dworkin, A. W. Schwartz and P. Ehrenfreund, *Earth Planet. Sci. Lett.*, 2008, **270**, 130–136.
- 38 R. K. Robins, *J. Am. Chem. Soc.*, 1958, **80**, 6671–6679.
- 39 S. Pizzarello and W. Holmes, *Geochim. Cosmochim. Acta*, 2009, **73**, 2150–2162.
- 40 D. S. N. Parker, R. I. Kaiser, B. Bandyopadhyay, O. Kostko, T. P. Troy and M. Ahmed, *Angew. Chem., Int. Ed.*, 2015, **54**, 5421–5424.
- 41 T. Yang, R. I. Kaiser, T. P. Troy, B. Xu, O. Kostko, M. Ahmed, A. M. Mebel, M. V. Zagidullin and V. N. Azyazov, *Angew. Chem., Int. Ed.*, 2017, **56**, 4515–4519.
- 42 F. Qi, *Proc. Combust. Inst.*, 2013, **34**, 33–63.
- 43 M. V. Zagidullin, R. I. Kaiser, D. Porfiriev, I. P. Zavershinskiy, M. Ahmed, V. N. Azyazov and A. M. Mebel, *J. Phys. Chem. A*, 2018, **122**, 8819–8827.
- 44 A. D. Becke, *J. Chem. Phys.*, 1993, **98**, 5648–5652.
- 45 C. Lee, W. Yang and R. G. Parr, *Phys. Rev. B: Condens. Matter Mater. Phys.*, 1988, **37**, 785–789.

- 46 L. A. Curtiss, K. Raghavachari, P. C. Redfern, V. Rassolov and J. A. Pople, *J. Chem. Phys.*, 1998, **109**, 7764–7776.
- 47 L. A. Curtiss, K. Raghavachari, P. C. Redfern, A. G. Baboul and J. A. Pople, *Chem. Phys. Lett.*, 1999, **314**, 101–107.
- 48 A. G. Baboul, L. A. Curtiss, P. C. Redfern and K. Raghavachari, *J. Chem. Phys.*, 1999, **110**, 7650–7657.
- 49 T. H. Dunning Jr, *J. Chem. Phys.*, 1989, **90**, 1007–1023.
- 50 J. M. Martin and O. Uzan, *Chem. Phys. Lett.*, 1998, **282**, 16–24.
- 51 G. Knizia, T. B. Adler and H.-J. Werner, *J. Chem. Phys.*, 2009, **130**, 054104.
- 52 T. B. Adler, G. Knizia and H.-J. Werner, *J. Chem. Phys.*, 2007, **127**, 221106.
- 53 S. Grimme, *J. Chem. Phys.*, 2006, **124**, 034108.
- 54 L. Goerigk and S. Grimme, *J. Chem. Theory Comput.*, 2011, **7**, 291–309.
- 55 S. Grimme, S. Ehrlich and L. Goerigk, *J. Comput. Chem.*, 2011, **32**, 1456–1465.
- 56 M. J. Frisch, G. W. Trucks, H. B. Schlegel, G. E. Scuseria, M. A. Robb, J. R. Cheeseman, G. Scalmani, V. Barone, B. Mennucci, G. A. Petersson, H. Nakatsuji, M. Caricato, X. Li, H. P. Hratchian, A. F. Izmaylov, J. Bloino, G. Zheng, J. L. Sonnenberg, M. Hada, M. Ehara, K. Toyota, R. Fukuda, J. Hasegawa, M. Ishida, T. Nakajima, Y. Honda, O. Kitao, H. Nakai, T. Vreven, J. A. Montgomery, Jr., J. E. Peralta, F. Ogliaro, M. Bearpark, J. J. Heyd, E. Brothers, K. N. Kudin, V. N. Staroverov, T. Keith, R. Kobayashi, J. Normand, K. Raghavachari, A. Rendell, J. C. Burant, S. S. Iyengar, J. Tomasi, M. Cossi, N. Rega, J. M. Millam, M. Klene, J. E. Knox, J. B. Cross, V. Bakken, C. Adamo, J. Jaramillo, R. Gomperts, R. E. Stratmann, O. Yazyev, A. J. Austin, R. Cammi, C. Pomelli, J. W. Ochterski, R. L. Martin, K. Morokuma, V. G. Zakrzewski, G. A. Voth, P. Salvador, J. J. Dannenberg, S. Dapprich, A. D. Daniels, O. Farkas, J. B. Foresman, J. V. Ortiz, J. Cioslowski and D. J. Fox, *Gaussian 09, revision A.02*, Gaussian Inc., CT, 2009.
- 57 H. J. Werner, P. J. Knowles, G. Knizia, F. R. Manby, M. Schütz, P. Celani, W. Györfy, D. Kats, T. Korona, R. Lindh, A. Mitrushenkov, G. Rauhut, K. R. Shamasundar, T. B. Adler, R. D. Amos, A. Bernhardsson, A. Berning, D. L. Cooper, M. J. O. Deegan, A. J. Dobbyn, F. Eckert, E. Goll, C. Hampel, A. Hesselmann, G. Hetzer, T. Hrenar, G. Jansen, C. Köppl, Y. Liu, A. W. Lloyd, R. A. Mata, A. J. May, S. J. McNicholas, W. Meyer, M. E. Mura, A. Nicklaß, D. P. O'Neill, P. Palmieri, D. Peng, K. Pflüger, R. Pitzer, M. Reiher, T. Shiozaki, H. Stoll, A. J. Stone, R. Tarroni, T. Thorsteinsson and M. Wang, *MOLPRO, version 2010.1*, University College Cardiff Consultants Ltd, UK, 2010, <http://www.molpro.net>.
- 58 P. J. Robinson and K. A. Holbrook, *Unimolecular reactions*, Wiley, New York, 1972.
- 59 H. Eyring and S. H. Lin, *Basic chemical kinetics*, John Wiley & Sons, Inc., 1980.
- 60 J. I. Steinfeld, J. S. Francisco and W. L. Hase, *Chemical kinetics and dynamics*, Prentice Hall, Upper Saddle River, NJ, 1999.
- 61 V. Kislov, T. Nguyen, A. Mebel, S. Lin and S. Smith, *J. Chem. Phys.*, 2004, **120**, 7008–7017.
- 62 J. Bouwman, A. Bodi and P. Hemberger, *Phys. Chem. Chem. Phys.*, 2018, **20**, 29910–29917.
- 63 R. M. C. Lopes, S. D. Wall, C. Elachi, S. P. D. Birch, P. Corlies, A. Coustenis, A. G. Hayes, J. D. Hofgartner, M. A. Janssen, R. L. Kirk, A. LeGall, R. D. Lorenz, J. I. Lunine, M. J. Malaska, M. Mastroguiseppe, G. Mitri, C. D. Neish, C. Notarnicola, F. Paganelli, P. Paillou, V. Poggiali, J. Radebaugh, S. Rodriguez, A. Schoenfeld, J. M. Soderblom, A. Solomonidou, E. R. Stofan, B. W. Stiles, F. Tosi, E. P. Turtle, R. D. West, C. A. Wood, H. A. Zebker, J. W. Barnes, D. Casarano, P. Encrenaz, T. Farr, C. Grima, D. Hemingway, O. Karatekin, A. Lucas, K. L. Mitchell, G. Ori, R. Orosei, P. Ries, D. Riccio, L. A. Soderblom and Z. Zhang, *Space Sci. Rev.*, 2019, **215**, 33.
- 64 M. Scherf, H. Lammer, N. V. Erkaev, K. E. Mandt, S. E. Thaller and B. Marty, *Space Sci. Rev.*, 2020, **216**, 123.
- 65 K. L. Kelvin Lee, R. A. Loomis, A. M. Burkhardt, I. R. Cooke, C. Xue, M. A. Siebert, C. N. Shingledecker, A. Remijan, S. B. Charnley, M. C. McCarthy and B. A. McGuire, *Astrophys. J.*, 2021, **908**, L11.
- 66 F. Zhang, P. Maksyutenko and R. I. Kaiser, *Phys. Chem. Chem. Phys.*, 2012, **14**, 529–537.
- 67 B. Sun, C. Huang, S. Chen, S. Chen, R. Kaiser and A. Chang, *J. Phys. Chem. A*, 2014, **118**, 7715–7724.
- 68 S. B. Morales, C. J. Bennett, S. D. Le Picard, A. Canosa, I. R. Sims, B. Sun, P. Chen, A. H. Chang, V. V. Kislov and A. M. Mebel, *Astrophys. J.*, 2011, **742**, 26.
- 69 S. Soorkia, C. A. Taatjes, D. L. Osborn, T. M. Selby, A. J. Trevitt, K. R. Wilson and S. R. Leone, *Phys. Chem. Chem. Phys.*, 2010, **12**, 8750–8758.
- 70 R. McCarroll, *AIP Conf. Proc.*, 2004, **740**, 3–19.
- 71 M. F. Lin, Y. A. Dyakov, C. M. Tseng, A. M. Mebel, S. H. Lin, Y. T. Lee and C. K. Ni, *J. Chem. Phys.*, 2005, **123**, 054309.
- 72 K. A. Prather and Y. T. Lee, *Isr. J. Chem.*, 1994, **34**, 43–53.
- 73 M. Lucas, A. M. Thomas, R. I. Kaiser, E. K. Bashkurov, V. N. Azyazov and A. M. Mebel, *J. Phys. Chem. A*, 2018, **122**, 3128–3139.